Divide and Conquer Interaction Energy Decomposition

Arjan van der Vaart and Kenneth M. Merz, Jr.*

Department of Chemistry, 152 Davey Laboratory, The Pennsylvania State University, University Park, Pennsylvania 16802

Received: November 20, 1998; In Final Form: February 23, 1999

We present a new energy decomposition scheme, which decomposes interaction energies into electrostatic, polarization, and charge transfer contributions. The method is founded on the divide and conquer approach but is only prone to errors introduced by the basis set and the applied Hamiltonian. We illustrate the method by AM1/PM3 interaction energy decompositions on bimolecular systems and 64 water systems. Our decomposition scheme also allows for screening of charge transfer or charge transfer and polarization from intermolecular interactions. Screening of these interactions is illustrated by the charge analysis of a screened 64 water system. Our calculations indicate the importance of charge transfer, even for intermolecular separations 0.5−1.0 Å from equilibrium.

Introduction

Modern simulation methods allow for the simulation of thousands of molecules.[1−3] Interactions between these molecules are conveniently handled by parametrized force fields, based on classical mechanics.[1] Most force fields represent the intermolecular interactions by a combination of electrostatics and Lennard-Jones forces. Force fields with explicit polarization[4−13] show that polarization accounts for up to ∼15% of the interaction energy.[4,13] Similar results have been obtained by quantum mechanical methods.[14,15] Although this amount is significant, polarization is usually omitted or treated in an average way through the proper choice of parameters, to avoid the computational expense of polarizable force fields.

Quantum mechanical phenomena, like reactivity and charge transfer, cannot be handled by classical methods. Charge transfer has been shown to be important in binary clusters of small compounds.[16] It has also been shown by quantum mechanical methods in our lab that as much as 2 units of charge are transferred between protein and water in solvated major cold shock protein A (CSPA).[17] These observations suggest that charge transfer may also be important for the energetics of solvated (bio-) molecular systems.

Progress to calculate the contributions of electrostatics, polarization, and charge transfer to the interaction energy has been made by Natural Bond Order (NBO) analysis[16,18,19] and Kitaura−Morokuma (KM) analysis.[20] These quantum mechanical methods work through the deletion of specific Fock matrix elements connecting filled and unfilled orbitals. In both methods, the orthogonalization of atomic orbitals to assess charge transfer is central. In NBO a weighted symmetric orthogonalization procedure assigns orbitals to monomers, based on a maximum occupancy criterion. Since the occupied orbitals resemble Lewis structures, this criterion sometimes leads to ambiguous results when resonant electronic structures are available, for example, in CO_2.[16] In KM, unoccupied orbitals are implicitly orthogonalized to the occupied orbitals of the other monomer. Most of the overlap between antibonding orbitals of the one monomer and occupied orbitals of the other monomer will be assigned to the occupied orbital. Part of the charge transfer energy term

will therefore be absorbed in the electrostatic energy contribution.[18] More importantly, neither method is easily implemented and the computational cost prohibits the treatment of large chemical systems.

We present a new method that decomposes the interaction energy into electrostatic, polarization, and charge transfer components. The method is an extension of an earlier decompostion approach that only incorporated polarization, using a continuum solvent model.[15] Our method is founded on the divide and conquer (D&C) method[21−23] and is readily implemented in existing D&C algorithms. The D&C method is a linear scaling quantum mechanical approach, which routinely allows calculation of large systems (up to 20 000 atoms). By division of the system into subsystems, diagonalization of the Fock matrix of the total system is replaced by diagonalization of several smaller matrixes in the most expensive part of the calculation. Charge flow between subsystems is controlled by subsystem overlap and by the Fermi energy. We exploit these features in our decomposition scheme to effectively screen interactions and inhibit charge flow between subsystems.

We tested our method on small bimolecular systems and on a 64 water system. Although the method is not limited to a particular Hamiltonian, only semiempirical AM1[24] and PM3[25−27] calculations were performed due to a lack of access to other D&C programs. We hope to extend our calculations soon to DFT methods to investigate the generality of our results.

Theory

The D&C method[21−23] divides a molecular system into overlapping subsystems. For each of these subsystems, α, the localized Roothaan−Hall equation

$$F^\alpha C^\alpha = S^\alpha C^\alpha E^\alpha \qquad (1)$$

is solved. Where C^α is the subsystem coefficient matrix, F^α is the subsystem Fock matrix, and E^α is the diagonal matrix of orbital energies for subsystem α. S^α is the overlap matrix, which is equal to the identity matrix for semiempirical Hamiltonians.

The local Fock matrix is built from the global Fock matrix:

$$F_{\mu\nu}^\alpha = \begin{cases} F_{\mu\nu} \text{ if the basis functions } \chi_\mu \text{ and } \chi_\nu \\ \qquad \text{ are in the same subsystem} \\ 0 \text{ otherwise} \end{cases} \quad (2)$$

The global Fock matrix is constructed from the one-electron matrix $H_{\mu\nu}$, the two-electron integrals $(\nu\nu|\lambda\sigma)$, and the global density matrix $P_{\mu\nu}$:

$$F_{\mu\nu} = H_{\mu\nu} + \sum_{\lambda=1}^{N}\sum_{\sigma=1}^{N}\left[(\mu\nu/\lambda\sigma) - \frac{1}{2}(\mu\sigma|\lambda\nu)\right]P_{\lambda\sigma} \quad (3)$$

Electron flow between subsystems is mediated through buffer regions and indirectly through the Fermi energy ϵ_F. The Fermi energy is determined iteratively subject to the constraint that the total number of electrons is conserved. With the Fermi energy, the occupation numbers n_i^α for each subsystem are calculated:

$$n_i^\alpha = \frac{2}{1 + \exp[(\epsilon_i^\alpha - \epsilon_F)/kT]} \quad (4)$$

where ϵ_i^α is the molecular orbital energy. Using these occupation numbers, the local density matrix for each subsystem α can be obtained from

$$P_{\mu\nu}^\alpha = \sum_i^{N^\alpha} n_i^\alpha (c_{\mu i}^\alpha) c_{\nu i}^\alpha \quad (5)$$

where N^α is the number of orbitals in subsystem α. Every subsystem consists of a core surrounded by two buffer layers.[23] These buffer regions are used to determine what information from the local density matrixes should be used to build the global density matrix:

$$P_{\mu\nu} = \sum_{\alpha=1}^{n_{sub}} D_{\mu\nu}^\alpha P_{\mu\nu}^\alpha \quad (6)$$

$$D_{\mu\nu}^\alpha = \begin{cases} 1/n_{\mu\nu} \text{ if } \chi_\mu \text{ is in the core and } \chi_\nu \text{ is in the core or} \\ \qquad\qquad \text{ inner buffer region (or vice versa)} \\ 0 \qquad \text{otherwise} \end{cases} \quad (7)$$

The total energy $E[\epsilon_F,P_r,r,b]$ of a multimolecular system is obtained from

$$E[\epsilon_F,P_r,r,b] = \frac{1}{2}\sum_\mu^M\sum_\nu^M (H_{\mu\nu} + F_{\mu\nu})P_{\mu\nu} + E_{core} \quad (8)$$

where M is the total number of basis functions and E_{core} is the core−core repulsion. From this point on, the total energy is expressed as a function of the Fermi energy, the intermolecular distance (r), the density matrix at this intermolecular distance (P_r), and the buffer region (b). The interaction energy of a multimolecular system can then be expressed as

$$E_{int} = E[\epsilon_F,P_r,r,b] - E[\epsilon_F,P_\infty,\infty,b] \quad (9)$$

The number of electrons per subsystem can be constrained by using multiple Fermi energies ϵ_F^α, instead of one global Fermi energy ϵ_F. Moreover, electron flow between subsystems can be inhibited by applying zero-buffering; that is, every subsystem consists only of a core. For an infinitely separated system, the buffer region will always be empty for any finite buffer region. Also, infinitely separated molecules do not interact with each other, meaning that intermolecular charge flow does not occur. Use of multiple Fermi energies will therefore give the same total energy as obtained by using one global Fermi energy:

$$E[\epsilon_F,P_\infty,\infty,b] = E[\epsilon_F^\alpha,P_\infty,\infty,0] \quad (10)$$

The electrostatic contribution to the interaction energy (E_{es}) can then be obtained from

$$E_{es} = E[\epsilon_F^\alpha,P_\infty,r,0] - E[\epsilon_F^\alpha,P_\infty,\infty,0] \quad (11)$$

Physically, this corresponds to the energy obtained by bringing the infinitely separated system to equilibrium distance, without a change in charge distribution. By allowing intramolecular charge rearrangement, the contribution of polarization to the interaction energy (E_{pol}) is obtained:

$$E_{pol} = E[\epsilon_F^\alpha,P_r,r,0] - E[\epsilon_F^\alpha,P_\infty,r,0] \quad (12)$$

The contribution of charge transfer to the interaction energy (E_{CT}) can be obtained by allowing intermolecular charge flow:

$$E_{CT} = E[\epsilon_F,P_r',r,b] - E[\epsilon_F^\alpha,P_r,r,0] \quad (13)$$

Errors in this interaction energy decomposition are introduced by the basis set, and the Hamiltonian used, and by the D&C approximation used in the calculation of $E[\epsilon_F,P_r,r,b]$. The latter can be eliminated by applying sufficiently large buffer regions or by performing a standard calculation, rather than a D&C calculation, to obtain $E[\epsilon_F,P_r,r,b]$.

Since $E_{int} = E_{es} + E_{pol} + E_{CT}$, only three calculations are needed to obtain all four terms. Moreover, $E[\epsilon_F^\alpha,P_\infty,r,0]$ can be obtained from the first SCF cycle in calculation of $E[\epsilon_F^\alpha,P_r,r,0]$, with P_∞ as the initial density matrix. Therefore, only three full SCF iterations need to be performed to obtain E_{int}, E_{es}, E_{pol}, and E_{CT}.

Results and Discussion

We implemented the interaction decomposition scheme in our D&C program (DivCon[22,23]) for the AM1[24] and PM3[25−27] Hamiltonians. We first performed the interaction decomposition on a series of bimolecular systems (Figure 1). The systems studied were water with acetate, ammonia, methylamine, methylammonium, dimethyl phosphate, the two-water system, and methylammonium with acetate. Water was studied both as hydrogen donor and acceptor in the ammonia−water and methylamine−water systems. Minimized configurations for these systems were obtained by AM1 and PM3-geometry optimizations. We also performed AM1 energy decompositions on the PM3 optimized configuration of the ammonia−water system, with ammonia as the hydrogen acceptor, and on the PM3-optimized configuration of the two-water system, since the AM1-optimized configurations of these systems show a bifurcated hydrogen bond pattern (Figure 1E,G).

Each subsystem consisted of one molecule, and the ϵ_F^α's were obtained in an iterative manner under the condition that every molecule had its formal charge. Since the systems are small, $E[\epsilon_F,P_r,r,b]$ was obtained by performing a standard AM1/PM3 calculation, rather than a D&C calculation.

We calculated the interaction energy curve for all bimolecular systems. These curves were obtained by performing the

Divide and Conquer Interaction Energy Decomposition

J. Phys. Chem. A, Vol. 103, No. 17, 1999 **3323**
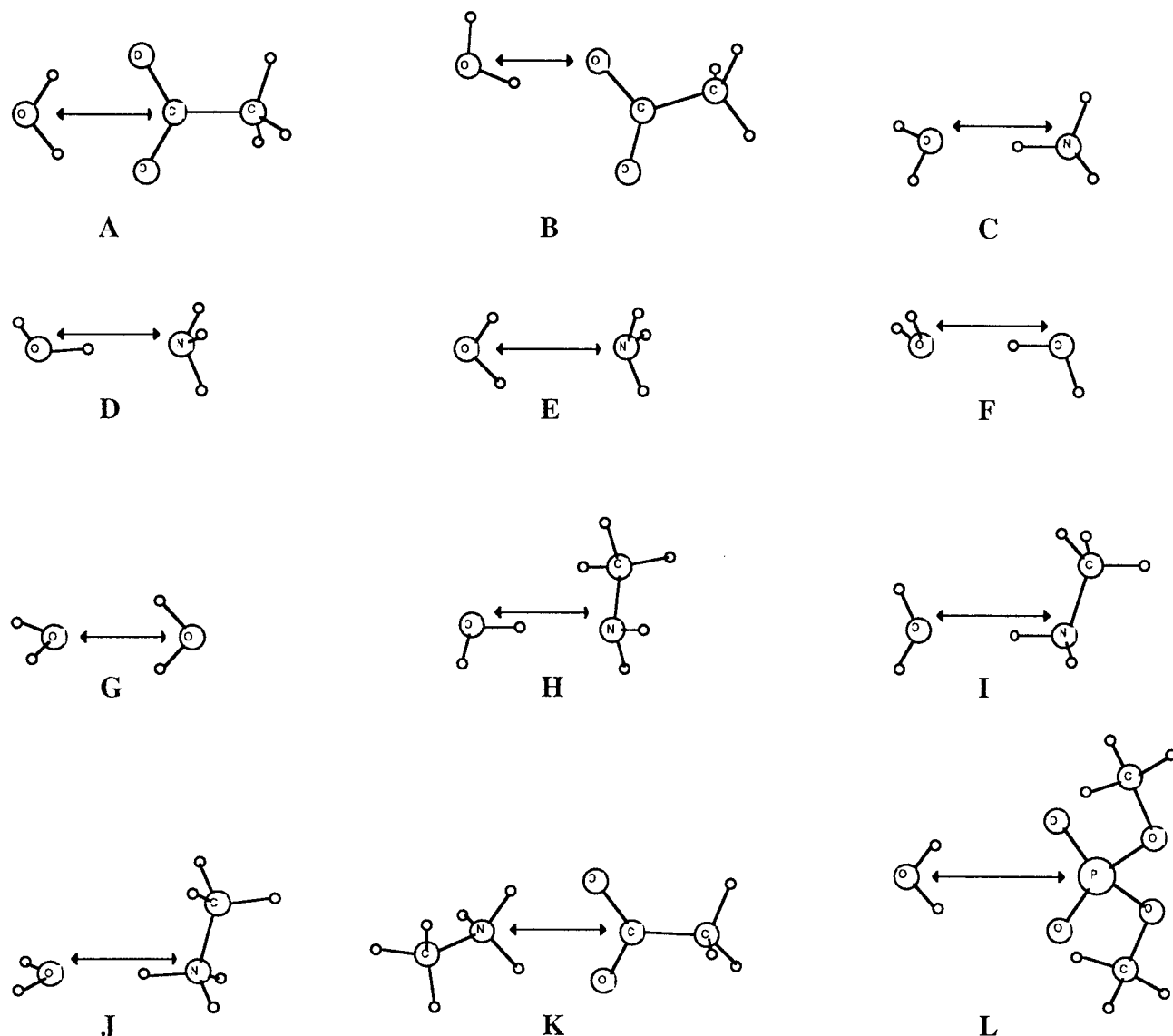
Figure 1. Configurations and intermolecular axis of the bimolecular systems studied: (A) acetate and water (this is the minimized AM1/PM3 geometry); (B) acetate and water, a local AM1/PM3 minimum; (C) ammonia and water, with ammonia as hydrogen donor (note that this is a local minimum); (D) ammonia and water, with ammonia as hydrogen acceptor, in the minimized PM3 geometry; (E) ammonia and water, with ammonia as hydrogen acceptor, in the minimized AM1 geometry; (F) two waters in the minimized PM3 geometry (this is a local minimum for AM1); (G) two waters in the minimized AM1 geometry; (H) methylamine and water, with water as hydrogen donor (this is the minimized structure for PM3, and a local minimum for AM1); (I) methylamine and water, with water as hydrogen acceptor (this is the minimized structure for AM1, and a local minimum for PM3); (J) methylammonium and water; (K) methylammonium and acetate; (L) dimethyl phosphate and water.

decomposition for several intermolecular distances along the intermolecular axis shown in Figure 1. Energy fractions for the electrostatic, polarization, and charge transfer contributions were also obtained. These fractions are defined as

$$\% \, E_x = \frac{100|E_x|}{|E_{es}| + |E_{pol}| + |E_{CT}|} \qquad x = es, \, pol, \, CT \quad (14)$$

The interaction energy curves and energy fractions for the acetate−water system of Figure 1A,B are shown in Figures 2 and 3, respectively. Graphs for the other systems are plotted in Figure 6S−15S.

For PM3, the interaction energy curves generally show wide shoulders and local minima at distances ∼1.0 Å larger than the equilibrium distances. This effect has been attributed to errors in the PM3 core repulsion function.[28] Since $E[\epsilon_F, P_r, r, b]$, $E[\epsilon_F^\alpha, P_r, r, 0]$, and $E[\epsilon_F^\alpha, P_\infty, r, 0]$ are all calculated at the same intermolecular separation r, the core−core repulsion of these

energies will be identical. Hence, the PM3 core repulsion terms will cancel in calculation of E_{pol} and E_{CT}. The errors in the PM3 core repulsion term will only have an effect on the electrostatic energy, since the core−core repulsion in $E[\epsilon_F^\alpha, P_\infty, \infty, 0]$ and $E[\epsilon_F^\alpha, P_\infty, r, 0]$ are different. Therefore, the PM3 electrostatic energy of distances ∼1.0 Å larger than the equilibrium distances will be erroneously lowered.

For all systems studied, polarization contributes only a small, stabilizing amount to the interaction energy. Polarization contributes maximally ∼6% to the interaction energy of the neutral molecules studied and maximally ∼7.5% to the systems with charged species. The notable exception is the acetate−water system in which water donates only one hydrogen bond (Figure 1B for the structure, Figure 3 for the interaction energy decomposition) with a maximum polarization contribution of 11.6% for AM1 at 2.625 Å separation and 12.4% for PM3 at 3.00 Å separation. Overall, for these small systems, polarization contributes slightly less than what is seen in condensed phases
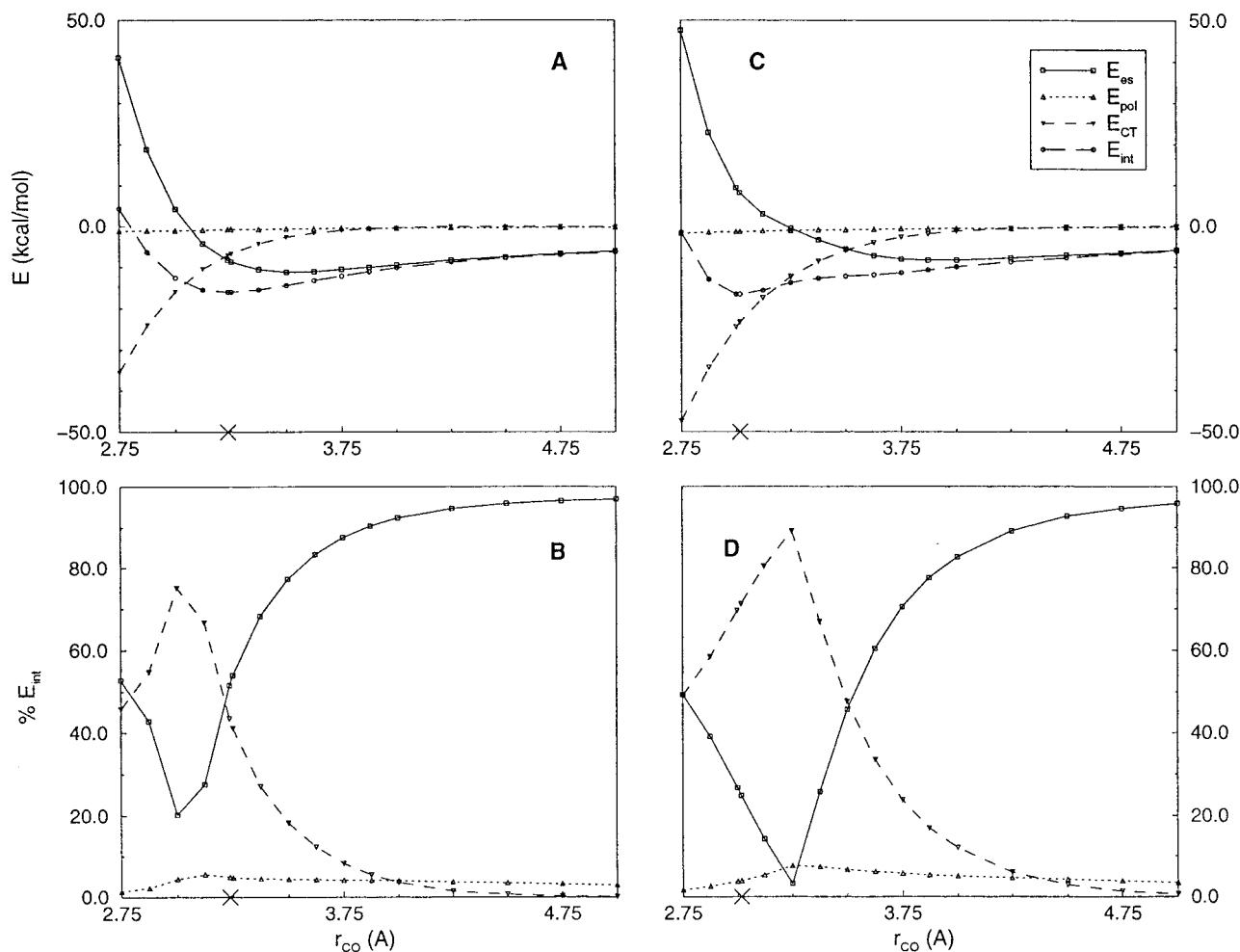
Figure 2. Interaction energy decomposition for acetate and water, with water donating two hydrogens, in the configuration of Figure 1A: (A) AM1 energies between 2.75 and 5.0 Å; (B) AM1 energy fractions between 2.75 and 5.0 Å; (C) PM3 energies between 2.75 and 5.0 Å; (D) PM3 energy fractions between 2.75 and 5.0 Å. The cross on the *x*-axis indicates the minimized geometry.

($\sim$10−15%),[14] but is in the same range as was observed for macromolecules in continuum solvent by York et al.[15]

The electrostatic contribution comprises $\sim$100% of the interaction energy at intermolecular distances larger than 6.0 Å (not shown in the figures). For PM3, the electrostatic energy is destabilizing at intermolecular distances smaller than and equal to the equilibrium separation, with the exception of the salt-bridged methylammonium−acetate system (Figures 1K and 14S). The electrostatic component of the interaction energy for AM1 is stabilizing at these distances, with the exception of the acetate−water system, in which water donates only one hydrogen bond (Figures 1B and 3) and the ammonia−water system in the PM3-minimized configuration (Figures 1D and 7S).

Charge transfer stabilizes the systems studied for every intermolecular separation. For distances smaller than the equilibrium distance, charge transfer constitutes a large fraction of the total interaction energy (40−90%), since the orbitals overlap strongly. Interestingly, charge transfer also constitutes a large fraction, more than 10%, of the interaction energy at equilibrium distance (Table 1) and distances up to 1.1 Å from equilibrium for AM1 and 1.7 Å for PM3 (Table 2). For AM1, the contribution of charge transfer to the interaction energy at equilibrium varies from 16.1% for the dimethyl phosphate−water system, to 76.5% for the acetate−water system in which water donates 1 hydrogen bond. Maximum intermolecular separations at which charge transfer still contributes 10% to

the interaction energies vary from 3.25 to 3.88 Å for AM1. Charge transfer is even more important in PM3: the contribution of charge transfer to the interaction energy at equilibrium varies between 31.0% for the methylammonium−acetate system, and 88.9% for the methylammonium−water system. The intermolecular separation at which charge transfer still accounts for 10% of the interaction energy varies from 3.63 to 4.50 Å for PM3.

The difference between the AM1 and PM3 results can be explained by the difference in treatment of hydrogen bonds by these methods. AM1 favors bifurcated structures with nonlinear O⋯H and N⋯H hydrogen bonds[29,30] (Table 3). This means that orbitals on the hydrogen atom interact less strongly with the heteroatom in a hydrogen bond for AM1 compared to PM3; hence charge transfer is less favorable in AM1.

As a second application, we performed an interaction energy decomposition of a 64 water system. Since AM1 favors bifurcated water structures[29,30] (Figure 1G), we decided to perform these calculations solely with the PM3 Hamiltonian. We obtained water configurations by performing a MD simulation for 330 ps on a cubix box of 64 TIP3P waters,[31] using the molecular dynamics package ROAR 1.0.[32] Temperature (300 K) and pressure (1 bar) were controlled with the Nosé−Hoover Chain algorithm,[33] and bond lengths and angles were constrained using the SHAKE algorithm.[34] We used a time step of 1.5 fs; the Ewald summation[1] was used for long-range electrostatic interactions, and periodic boundary conditions were in effect. Snapshots of the water system were taken at 210, 270, and 330

Divide and Conquer Interaction Energy Decomposition

J. Phys. Chem. A, Vol. 103, No. 17, 1999 **3325**
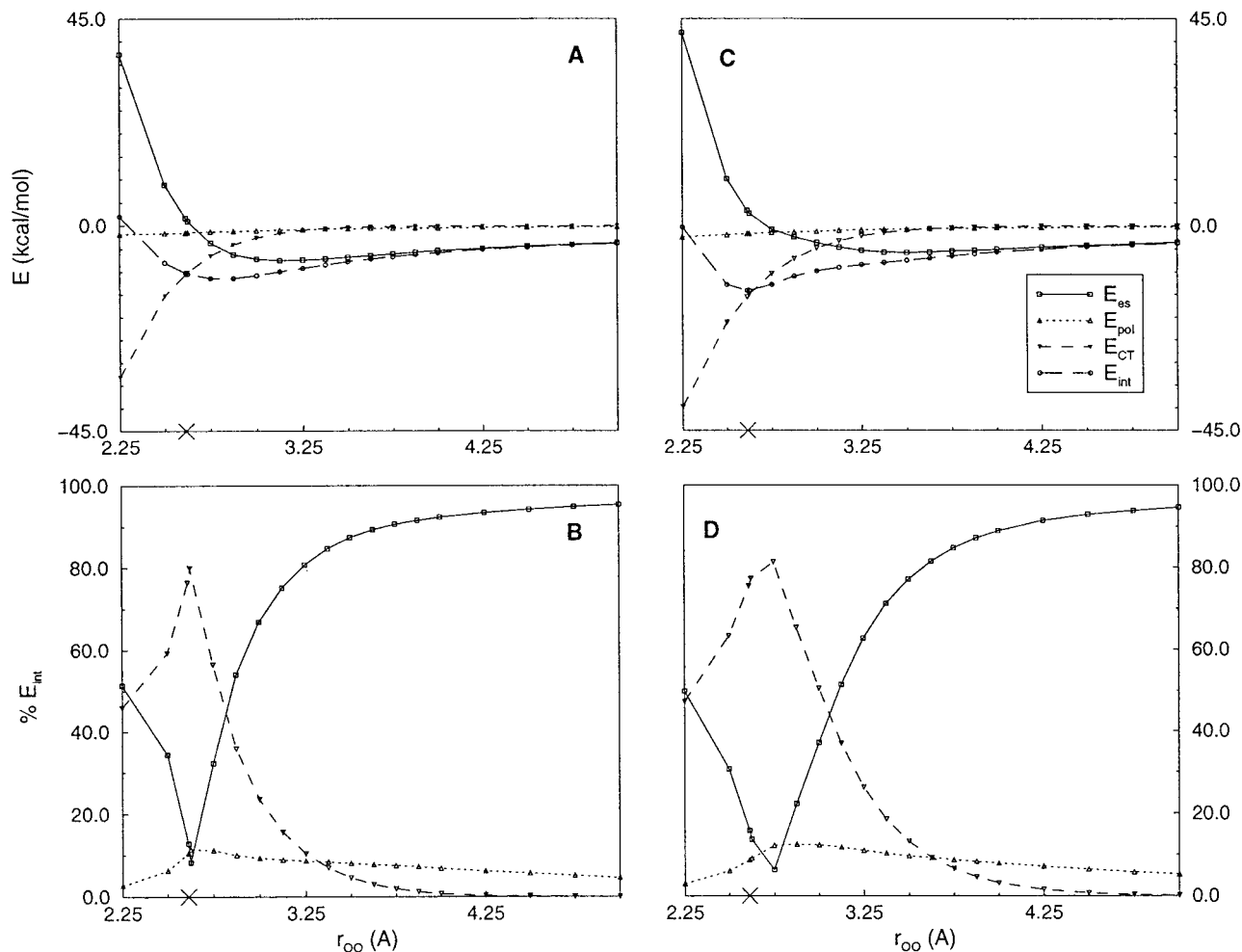
Figure 3. Interaction energy decomposition for acetate and water, with water donating one hydrogen, in the configuration of Figure 1B: (A) AM1 energies between 2.25 and 5.0 Å; (B) AM1 energy fractions between 2.25 and 5.0 Å; (C) PM3 energies between 2.25 and 5.0 Å; (D) PM3 energy fractions between 2.25 and 5.0 Å. The cross on the *x*-axis indicates the minimized geometry.

TABLE 1: Contribution of Charge Transfer to the Interaction Energy at the Equilibrium Separation

system	figure	r_{eq}^{AM1} (Å)[a]	r_{eq}^{PM3} (Å)[a]	% E_{CT}^{AM1} [b]	% E_{CT}^{PM3} [b]
acetate−water	1A	3.2351	3.0186	43.5	71.2
acetate−water	1B	2.6106	2.6106	76.5	75.4
ammonia−water	1C	3.0806	2.8637	63.7	52.0
ammonia−water	1D	2.7950	2.7950	47.1	55.8
ammonia−water	1E	3.1193		29.6	
water−water	1F	3.0596	2.7687	74.1	58.7
water−water	1G	2.6062		66.5	
methylamine−water	1H	3.5022	2.8077	31.6	54.9
methylamine−water	1I	3.0874	2.8581	71.8	51.7
methylammonium−water	1J	2.9871	2.7900	35.1	88.9
methylammonium−acetate	1K	3.0880	3.0005	21.7	31.0
dimethyl phosphate−water	1L	3.7336	3.1230	16.1	56.6

[a] Equilibrium separation. [b] Fraction of interaction energy.

ps. We placed one molecule in each subsystem for the interaction energy decomposition and constrained the charge on each subsystem to zero. To calculate $E[\epsilon_F^\alpha, P_\infty, \infty, 0]$, each molecule was placed on a grid point of a $4 \times 4 \times 4$ grid with grid spacing of 10^6 Å. A standard PM3 calculation was performed to obtain $E[\epsilon_F, P_r, r, b]$, and periodic boundary conditions were used throughout our calculations. Decompositions were performed on the MD snapshots and on PM3 geometry-optimized MD snapshots.

Results for the decomposition are listed in Table 4. The magnitude of each of the energy terms increases upon geometry optimization and the magnitude of the charge transfer contribution increases slightly more than the electrostatic contribution.

Both for PM3-optimized and -nonoptimized configurations, the electrostatic energy contributes ∼40% and charge transfer ∼60% to the interaction energy. Polarization accounts for about 1.5% of the interaction energy.

In Figure 4 the distribution of oxygen and hydrogen CM1[35] charges for the PM3-optimized systems are shown at every step of our decomposition. We choose to graph CM1 charges, rather than Mulliken charges, since CM1 charges provide a more accurate representation of the dipole moment.[35] Parts A and B of Figure 4 show the charge distributions after calculation of $E[\epsilon_F^\alpha, P_\infty, \infty, 0]$ and $E[\epsilon_F^\alpha, P_\infty, r, 0]$ (these charges are identical). This charge distribution corresponds to the charge distribution of a system in which the intermolecular interactions are solely

TABLE 2: Maximum Intermolecular Separation at Which Charge Transfer Constitutes 10% of the Interaction Energy

system	figure	r_{10}^{AM1} (Å)[a]	r_{10}^{PM3} (Å)[a]	Δr_{10}^{AM1} (Å)[b]	Δr_{10}^{PM3} (Å)[b]
acetate−water	1A	3.75	4.00	0.51	0.98
acetate−water	1B	3.25	3.63	0.64	1.01
ammonia−water	1C	3.75	4.50	0.67	1.64
ammonia−water	1D	3.88	4.50	1.08	1.71
ammonia−water	1E	3.50		0.38	
water−water	1F	3.75	4.25	0.69	1.48
water−water	1G	3.25		0.64	
methylamine−water	1H	3.88	4.50	0.37	1.69
methylamine−water	1I	3.75	4.50	0.66	1.64
methylammonium−water	1J	3.38	3.63	0.39	0.84
methylammonium−acetate	1K	3.38	3.50	0.29	0.50
dimethyl phosphate−water	1L	3.88	4.25	0.14	1.13

[a] Maximum intermolecular separation at which charge transfer constitutes 10% of the interaction energy. [b] Distance from equilibrium at which charge transfer constitutes 10% of the interaction energy.

TABLE 3: Comparison of Hydrogen Bond Geometries at Equilibrium[a]

system	figure	angle	AM1[b]	PM3[b]	bond	AM1[c]	PM3[c]
acetate−water	1A	O−H⋯O	140.5	139.1	H⋯O	2.04	1.82
			137.9	139.0		2.04	1.82
ammonia−water	1C	N−H⋯O	151.2	168.8	H⋯O	2.17	1.87
water−water	1F	O−H⋯O	176.6	179.2	H⋯O	2.10	1.81
methylamine−water	1H	O−H⋯N	154.5	179.7	H⋯N	2.61	1.84
methylamine−water	1I	N−H⋯O	173.9	175.7	H⋯O	1.96	1.78
methylammonium−water	1J	N−H⋯O	151.8	168.5	H⋯O	2.17	1.86
methylammonium−acetate	1K	N−H⋯O	138.1	136.5	H⋯O	1.79	1.71
			137.5	136.6		1.80	1.71
dimethyl phosphate−water	1L	O−H⋯O	140.6	124.4	H⋯O	2.44	2.02
			140.8	144.8		2.44	1.84

[a] The configurations of acetate−water, with water donating only one hydrogen bond (Figure 1B), and ammonia−water, with ammonia as hydrogen acceptor (Figure 1D), have been omitted, since these structures are identical for the AM1 and PM3 calculations. The AM1 configurations of the ammonia−water system, with ammonia as hydrogen acceptor (Figure 1E), and the biwater system (Figure 1G) have been omitted, since no PM3 calculations were performed on these configurations. [b] In degrees. [c] In Å.

TABLE 4: Interaction Energy Decomposition of 64 Waters

time (ps)	opt[a]	E_{int}[b]	E_{es}[b]	E_{pol}[b]	E_{CT}[b]	% E_{es}	% E_{pol}	% E_{CT}
210	no	−225.75	485.70	−17.75	−693.70	40.6	1.5	57.9
270	no	−180.54	607.89	−15.64	−772.79	43.5	1.1	55.4
330	no	−221.38	476.55	−17.07	−680.86	40.6	1.4	58.0
210	yes	−385.73	622.62	−27.52	−980.83	38.2	1.7	60.1
270	yes	−380.00	622.56	−26.26	−976.30	38.3	1.6	60.1
330	yes	−389.60	592.54	−26.95	−955.19	37.6	1.7	60.7

[a] Yes if a PM3 geometry optimization was performed. [b] In kcal/mol.

formed by electrostatics. Parts C and D of Figure 4 show the charge distributions after calculation of $E[\epsilon_F^\alpha, P_r, r, 0]$, which corresponds to the charge distribution of a system in which the intermolecular interactions are formed by a combination of electrostatics and polarization. Finally, parts E and F of Figure 4 show the charge distributions after calculation of $E[\epsilon_F, P_r, r, b]$, corresponding to the charge distribution of a system in which the intermolecular interactions also include charge transfer. In Figure 16S, analogous graphs are plotted for the nonoptimized systems.
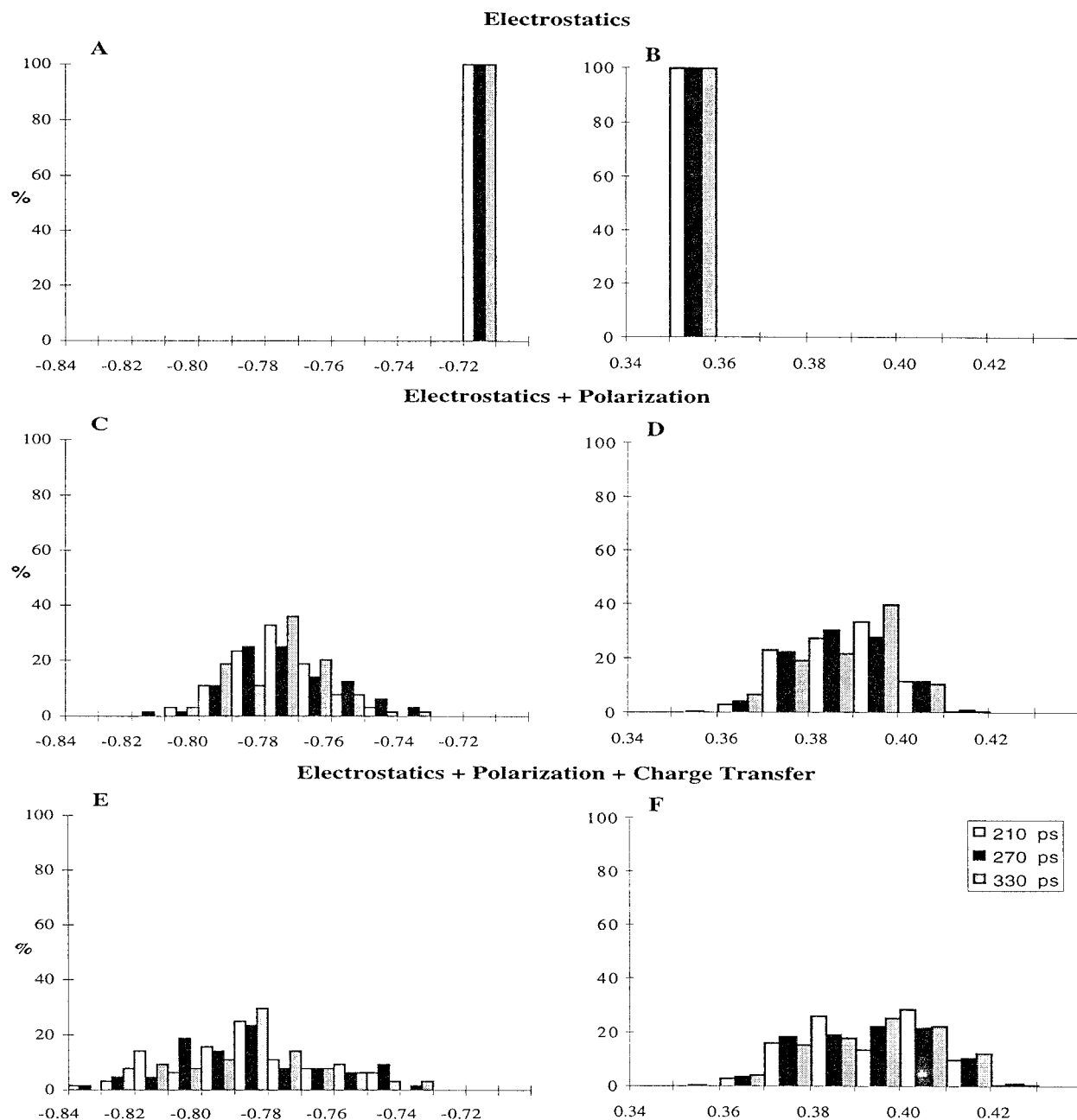
The charge distribution of a water system in which the intermolecular interactions consist of electrostatics only is a delta function. Polarization transforms this distribution into a bell-shaped one, thereby shifting the mean of the distribution to higher absolute values. Charge transfer flattens this distribution, shifting the mean to slightly higher absolute values. This effect is observed for both the optimized and nonoptimized systems, the optimized system having slightly higher charged atoms than the nonoptimized system.

Figure 4 suggests that polarization has a more dramatic effect on atomic charge rearrangement than charge transfer. Indeed, the charge on each atom changes more through the addition of

polarization to electrostatics than in adding charge transfer to electrostatics and polarization, as shown in Figure 5. Figure 5A graphs the distribution of oxygen atom charge differences between charges obtained in calculating $E[\epsilon_F^\alpha, P_r, r, 0]$ and $E[\epsilon_F^\alpha, P_\infty, r, 0]$. This distribution represents the charge difference on oxygen atoms in adding polarization to the electrostatic interaction. Figure 5C plots the distribution of oxygen atom charge differences between charges from $E[\epsilon_F^\alpha, P_r, r, b]$ and $E[\epsilon_F^\alpha, P_r, r, 0]$, representing the charge difference in adding charge transfer to electrostatics and polarization. In Figure 5B,D the same is done for the hydrogen charges. Figure 5 is for the PM3-optimized configurations; Figure 17S, for the nonoptimized configurations.

Parts C and D of Figure 5 show that the charge difference distribution in adding charge transfer to electrostatics and polarization is peaked around zero, especially for the nonoptimized configurations (Figure 17S). Moreover, this distribution is relatively sharp, in comparison to Figure 5A,B, especially for the hydrogen atoms. This means that the charge on each individual atom does not change much in adding charge transfer to the electrostatic and polarization interactions. Adding polarization to purely electrostatic interactions (Figure 5A,B) changes these individual charges more: the mean for oxygen is ∼−0.06 charge units, for hydrogen ∼0.02 charge units.

Although atomic charges change more in adding polarization to electrostatics, than in adding charge transfer to electrostatics and polarization, energetically the latter is far more favorable. This can be seen in Table 4, where polarization only accounts for ∼1.5% of the interaction energy and charge transfer ∼60%. Intramolecular electron rearrangement (i.e., polarization) appears to be relatively facile, but the net increase in the interaction energy, in our case, appears to be relatively small. This

Divide and Conquer Interaction Energy Decomposition

J. Phys. Chem. A, Vol. 103, No. 17, 1999 **3327**

Electrostatics

Electrostatics + Polarization

Electrostatics + Polarization + Charge Transfer

Figure 4. Effect of electrostatics, polarization, and charge transfer on the oxygen and hydrogen CM1 charge distribution of the PM3 optimized, 64 water system: (A) Oxygen charge distribution, $E_{int} = E_{es}$, $E_{pol} = E_{CT} = 0$; (B) hydrogen charge distribution, $E_{int} = E_{es}$, $E_{pol} = E_{CT} = 0$; (C) oxygen charge distribution, $E_{int} = E_{es} + E_{pol}$, $E_{CT} = 0$; (D) hydrogen charge distribution, $E_{int} = E_{es} + E_{pol}$, $E_{CT} = 0$; (E) oxygen charge distribution, $E_{int} = E_{es} + E_{pol} + E_{CT}$; (F) hydrogen charge distribution, $E_{int} = E_{es} + E_{pol} + E_{CT}$.

observation is in agreement with NBO studies using ab initio methods by Reed et al.[16] Charge transfer appears to have a smaller effect on the intramolecular electron distribution. Despite this, the net transfer of charge from one monomer to another has a large effect on the total interaction energy, which, again, is in agreement with NBO results.[16]

Conclusion

We presented a new method that decomposes the interaction energy of any system into electrostatic, polarization, and charge transfer contributions. The method is grounded in a divide and conquer approach but only introduces errors related to the basis set and Hamiltonian used. We performed a series of test calculations on bimolecular systems and a 64 water system, using the AM1 and PM3 Hamiltonian. Within the limitations

of these Hamiltonians, we observed that charge transfer contributes a significant fraction to the interaction energy of all systems studied. This contribution is not only significant when intermolecular distances are small, but also at equilibrium distances, where it accounts for between ~15 and ~90% of the interaction energy. Even at distances 0.5−1.0 Å from equilibrium, charge transfer is energetically still significant, comprising ~10% of the interaction energy.

Our method also allows the screening of either charge transfer or charge transfer and polarization from the intermolecular interactions. This makes a detailed study of the effect of electrostatics, polarization, and charge transfer on the charge distributions of the system of interest possible. We illustrated this approach by analysis of the effect of polarization and charge transfer on a system of 64 waters. Polarization has a dramatic

Polarization - Electrostatics

Charge Transfer - Polarization
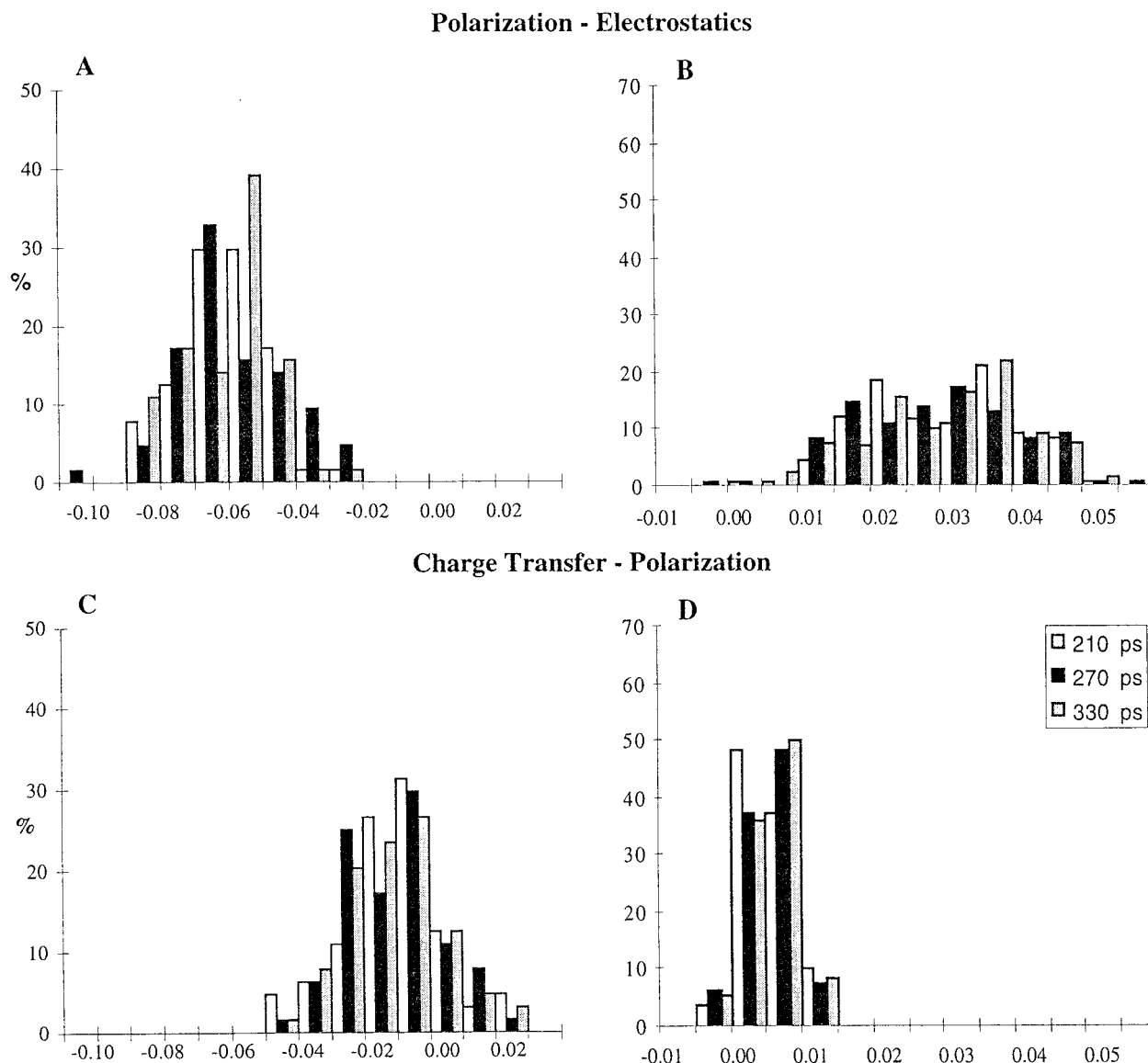
Figure 5. Distribution of CM1 charge differences per oxygen/hydrogen atom on inclusion of polarization and charge transfer for the PM3-optimized, 64 water system: (A) distribution of the charge difference on oxygen atoms in adding polarization to the electrostatic interaction; (B) distribution of the charge difference on hydrogen atoms in adding polarization to the electrostatic interaction; (C) distribution of the charge difference on oxygen atoms in adding charge transfer to the electrostatic + polarization interaction; (D) Distribution of the charge difference on hydrogen atoms in adding charge transfer to the electrostatic + polarization interaction.

effect on the atomic charge rearrangement of water and creates a bell-shaped charge distribution with higher charges than the delta-shaped charge distribution of a pure electrostatic system. Charge transfer has less of an impact, flattening and shifting the distribution slightly to higher charges.

The divide and conquer framework of our approach will allow interaction decompositions on large systems, like solvated proteins. We expect this approach to be very useful in obtaining a more detailed understanding of the complex role of solvation in the energetics and charge distributions of biomolecular systems.

References and Notes

(1) Allen, M. P.; Tildesley, D. J. *Computer Simulation of Liquids*; Clarendon Press: Oxford, U.K., 1987.

(2) Lybrand, T. P. Computer Simulation of Biomolecular Systems Using Molecular Dynamics and Free Energy Peturbation Methods. *Rev. Comput. Chem.* **1990**, *1*, 295−320.

(3) van Gunsteren, W. F.; Berendsen, H. J. C. Computer Simulation of Molecular Dynamics: Methodology, Applications and Perspectives in Chemistry. *Angew. Chem., Int. Ed. Engl.* **1990**, *29*, 992−1023.

(4) Kuwajima, S.; Warshel, A. Incorporating Electric Polarizabilities in Water−Water Interaction Potentials. *J. Phys. Chem.* **1990**, *94*, 460−466.

(5) Applequist, J.; Carl, J. R.; Fung, K. K. An Atom Dipole Interaction Model for Molecular Polarizability. Application to Polyatomic Molecules and Determination of Atom Polarizabilities. *J. Am. Chem. Soc.* **1972**, *94*, 2952−2960.

(6) Applequist, J. Atom Charge Transfer in Molecular Polarizabilities. Application of the Olson-Sundberg Model to Aliphatic and Aromatic Hydrocarbons. *J. Phys. Chem.* **1993**, *97*, 6016−6023.

(7) Dang, L. X.; Rice, J. E.; Caldwell, J.; Kollman, P. A. Ion Solvation in Polarizable Water: Molecular Dynamics Simulations. *J. Am. Chem. Soc.* **1991**, *113*, 2481.

(8) Rick, S. W.; Stuart, S. J.; Berne, B. J. Dynamical Fluctuating Charge Force Fields: Application to Liquid Water. *J. Chem. Phys.* **1994**, *101*, 6141−6156.

(9) New, M. H.; Berne, B. J. Molecular Dynamics Calculation of the Effect of Solvent Polarizability on the Hydrophobic Interaction. *J. Am. Chem. Soc.* **1995**, *117*, 7172−7179.

(10) Stuart, S. J.; Berne, B. J. Effects of Polarizability on the Hydration of the Chloride Ion. *J. Phys. Chem.* **1996**, *100*, 11934−11943.

(11) Caldwell, J.; Dang, L. X.; Kollman, P. A. Implementation of Nonadditive Intermolecular Potentials by Use of Molecular Dynamics: Development of a Water−Water Potential and Water-Ion Cluster Interactions. *J. Am. Chem. Soc.* **1990**, *112*, 9144−9147.

(12) Wallqvist, A.; Ahlstrom, P.; Karlstrom, G. A new Intermolecular Energy Calculation Scheme: Applications to Potential Surface and Liquid Properties of Water. *J. Phys. Chem.* **1990**, *94*, 1649−1656.

(13) Gao, J. Absolute Free Energy of Solvation from Monter Carlo Simulations Using Combined Quantum and Molecular Mechanical Potentials. *J. Phys. Chem.* **1992**, *96*, 537−540.

(14) Gao, J.; Xia, X. A Priori Evaluation of Aqueous Polarization Effects Through Monte Carlo QM-MM Simulations. *Science* **1992**, *258*, 631−635.

(15) York, D. M.; Lee, T. S.; Yang, W. Quantum Mechanical Study of Aqueous Polarization Effects on Biological Macromolecules. *J. Am. Chem. Soc.* **1996**, *118*, 10940−10941.

(16) Reed, A. E.; Weinhold, F.; Curtiss, L. A.; Pochatko, D. J. Natural Bond Orbital Analysis of Molecular Interactions: Theoretical Studies of Binary Complexes of HF, H$_2$O, NH$_3$, N$_2$, O$_2$, F$_2$, CO, and CO$_2$ with HF, H$_2$O, and NH$_3$. *J. Chem. Phys.* **1986**, *84*, 5687−5705.

(17) Nadig, G.; van Zant, L. C.; Dixon, S. L.; Merz, K. M., Jr. Charge Transfer Interactions in Macromolecular Systems: A New View of the Protein/Water Interface. *J. Am. Chem. Soc.* **1998**, *120*, 5593−5594.

(18) Reed, A. E.; Curtiss, L. A.; Weinhold, F. Intermolecular Interactions from a Natural Bond Orbital, Donor−Acceptor Viewpoint. *Chem. Rev.* **1988**, *88*, 899−926.

(19) Weinhold, F. Nature of H−Bonding in Clusters, Liquids, and Enzymes: An Ab Initio, Natural Bond Orbital Perspective. *J. Mol. Struct.* **1997**, *399*, 181−197.

(20) Kitaura, K.; Morokuma, K. A New Energy Decomposition Scheme for Molecular Interactions within the Hartree−Fock Approximation. *Int. J. Quantum Chem.* **1976**, *10*, 325−340.

(21) Yang, W.; Lee, T.-S. A Density-Matrix Form of the Divide-and-Conquer Approach for Electronic Structure Calculations of Large Molecules. *J. Chem. Phys.* **1995**, *103*, 5674−5678.

(22) Dixon, S. L.; Merz, K. M., Jr. Semiempirical Molecular Orbital Calculations with Linear System Size Scaling. *J. Chem. Phys.* **1996**, *104*, 6643−6649.

(23) Dixon, S. L.; Merz, K. M., Jr. Fast, Accurate Semiempirical Molecular Orbital Calculations for Macromolecules. *J. Chem. Phys.* **1997**, *107*, 879−893.

(24) Dewar, M. J. S.; Zoebisch, E. G.; Healy, E. F.; Stewart, J. J. P. AM1: A New General Purpose Quantum Mechanical Molecular Model. *J. Am. Chem. Soc.* **1985**, *107*, 3902−3909.

(25) Stewart, J. J. P. Optimization of Parameters for Semiempirical Methods I. Method. *J. Comput. Chem.* **1989**, *10*, 209−220.

(26) Stewart, J. J. P. Optimization of Parameters fo Semiempirical Methods II. Applications. *J. Comput. Chem.* **1989**, *10*, 221−264.

(27) Stewart, J. J. P. Optimization of Parameters for Semiempirical Methods. III Extension of PM3 to Be, Mg, Zn, Ga, Ge, As, Se, Cd, In, Sn, Sb, Te, Hg, Tl, Pb and Bi. *J. Comput. Chem.* **1991**, *12*, 320−341.

(28) Csonka, G. I.; Angyan, J. G. The Origin of the Problems with the PM3 Core Repulsion Function. *J. Mol. Struct.* **1997**, *393*, 31−38.

(29) Zheng, Y. J.; Merz, K. M. J. Study of Hydrogen Bonding Interactions Relevant to Protein Structure and Function. *J. Comput. Chem.* **1992**, *13*, 1151−1169.

(30) Dannenberg, J. J. Hydrogen Bonds: A Comparison of Semiempirical and Ab Initio Treatments. *J. Mol. Struct.* **1997**, *401*, 279−286.

(31) Jorgensen, W. L.; Chandrasekhar, J.; Madura, J.; Impey, R. W.; Klein, M. L. Comparison of Simple Potential Functions for the Simulation of Liquid Water. *J. Chem. Phys.* **1983**, *79*, 926.

(32) Cheng, A.; Stanton, R. S.; Vincent, J. J.; Damodaran, K. V.; Dixon, S. L.; Hartsough, D. S.; Best, S. A.; Merz, K. M. J. ROAR; 1.0 ed.: The Pennsylvania State University: College Station, PA, 1997.

(33) Cheng, A.; Merz, K. M., Jr. Application of the Nose-Hoover Chain Method to the Study of Protein Dynamics. *J. Phys. Chem.* **1996**, *100*, 1927−1937.

(34) Ryckaert, J. P.; Ciccotti, G.; Berendsen, H. J. C. Numerical Integration of the Cartesian Equations of Motion of a System with Constraints: Molecular Dynamics of N−Alkanes. *J. Comput. Phys.* **1977**, *23*, 327−341.

(35) Storer, J. W.; Giesen, D. J.; Cramer, C. J.; Truhlar, D. G. Class IV Charge Models: A New Semiempirical Approach in Quantum Chemistry. *J. Comput.-Aided Mol. Design* **1995**, *9*, 87−110.